1

Advances in Aerodynamic Shape Optimization

Antony Jameson[1]

Stanford University, Stanford, CA 94305-4035
jameson@baboon.stanford.edu

1.1 Introduction

The focus of CFD applications has shifted to aerodynamic design. This shift has been mainly motivated by the availability of high performance computing platforms and by the development of new and efficient analysis and design algorithms. In particular automatic design procedures, which use CFD combined with gradient-based optimization techniques, have had a significant impact on the design process by removing difficulties in the decision making process faced by the aerodynamicist.

A fast way of calculating the accurate gradient information is essential since the gradient calculation can be the most time consuming portion of the design algorithm. The computational cost of gradient calculation can be dramatically reduced by the control theory approach since the computational expense incurred in the calculation of the complete gradient is effectively *independent* of the number of design variables. The foundation of control theory for systems governed by partial differential equations was laid by J.L. Lions [1]. The method was first used for aerodynamic design by Jameson in 1988 [2, 3]. Since then, the method has even been successfully used for the aerodynamic design of complete aircraft configurations [4].

In the present work a continuous adjoint formulation has been used to derive the adjoint system of equations, in which the adjoint equations are derived directly from the governing equations and then discretized. This approach has the advantage over the discrete adjoint formulation in that the resulting adjoint equations are independent of the form of discretized flow equations. The adjoint system of equations has a similar form to the governing equations of the flow, and hence the numerical methods developed for the flow equations [5, 6, 7] can be reused for the adjoint equations. Moreover, the gradient can be derived directly from the adjoint solution and the surface motion, independent of the mesh modification.

In order to accelerate the convergence of the descent process the gradient is then smoothed implicitly via a second order differential equation. This is

equivalent to redefining the gradient in a Sobolve space. The resulting procedure is very efficient, often yielding the optimum in 10-20 design cycles.

Recently wing planform parameters have been included as design variables and the Aerospace Computing Laboratory at Stanford University has successfully designed a wing which produces a specified lift with minimum drag, while meeting other criteria such as low structure weight, sufficient fuel volume, and stability and control [8]. Based on the promising results from our wing planform optimization strategy applied to inviscid flow and from our viscous aerodynamic design techniques [9, 10], we are now applying wing shape and planform optimization methods to viscous flow in order to take into account the viscous effects such as shock/boundary layer interaction, flow separation, and skin friction and eventually produce more realistic designs [11].

Additionally, the design method, which is greatly accelerated by the use of control theory, has been further enhanced by the use of a new continuous adjoint method, which reduce the volume integral part of the adjoint gradient formula to a surface integral [12], thus eliminating the dependence of the gradient formulas on the mesh perturbation. The computational savings in the gradient calculation are particularly significant for three-dimensional aerodynamic shape optimization problems on general unstructured and overset meshes. The use of unstructured grid techniques hold considerable promise for aerodynamic design by facilitating the treatment of complex configurations without incurring a prohibitive cost and bottleneck in mesh generation. The computational feasibility of using unstructured meshes for design is essentially enabled by the use of the continuous adjoint approach and the reduced gradient formulas [13]. Representative calculations are displayed in figures 1.2 through 1.6.

1.2 Adjoint and gradient formulations for the equations of transonic flow

The adjoint method may be applied directly to the partial differential equations to derive a continuous adjoint equation, which must then be discretized to obtain a numerical solution. Alternatively one may derive a discrete adjoint equation directly after first discretizing the flow equations. In this work the first procedure has been adopted because it allows more flexibility in the formulation of the gradient.

The procedure is illustrated here for the Euler equations. These are represented in transformed coordinates ξ_i on a fixed computational domain. Let

$$S = JK^{-1}$$

where

$$K_{ij} = \frac{\partial x_i}{\partial \xi_j}, J = det(K)$$

Then the transformed equations are

$$\frac{\partial F_i}{\partial \xi_i} = \frac{\partial (S_{ij} f_j)}{\partial \xi_i} = 0$$

As an example, consider the case of an inverse problem where one wishes to find the shape which brings the pressure as close as possible to the specified target pressure, p_t. Hence we try to minimize the cost function

$$\mathcal{I} = \frac{1}{2} \int_{\mathcal{B}} (p - p_t)^2 dS$$

over the design surface $\mathcal{B}$, which for convenience is assumed to be the surface $\psi_2 = 0$. Now a shape modification induces a change δp in the pressure and consequently

$$\delta \mathcal{I} = \int_{\mathcal{B}} (p - p_t) \delta p dS + \frac{1}{2} \int_{\mathcal{B}} (p - p_t)^2 d\delta S$$

Also the change in the solution is given by

$$\frac{\partial}{\partial \psi_i} \left(\delta F_i(w) \right) = 0$$

Here the flux changes are

$$\delta F_i = \delta S_{ij} f_j + C_i \delta w$$

where

$$C_i = S_{ij} \frac{\partial f_j}{\partial w}$$

Consequently one can augment the cost variation by

$$\int_{\mathcal{D}} \psi^T \frac{\partial \delta F_i}{\partial \xi_i} d\xi = \int_{\mathcal{B}} n_i \psi^T \delta F_i d\xi_{\mathcal{B}} - \int_{\mathcal{D}} \frac{\partial \psi^T}{\partial \xi} \delta F_i d\xi$$

Now choose ψ to satisfy the adjoint equation

$$C_i^T \frac{\partial \psi}{\partial \xi_i} = 0$$

with the boundary condition

$$\psi_2 \eta_x + \psi_3 \eta_y + \psi_4 \eta_z = p - p_t$$

where η_x, η_y, η_z are the components of the surface normal. Then the boundary integrals involving δp and the field integral involving δw are eliminated and the gradient is reduced to

$$\frac{1}{2} \int_{\mathcal{B}} (p - p_t)^2 d\delta S - \int \int_{\mathcal{B}} \left(\delta S_{21} \psi_2 + \delta S_{22} \psi_3 + \delta S_{23} \psi_4 \right) p d\xi_1 d\xi_3$$

$$-\int_{\mathcal{D}} \frac{\partial \psi^T}{\partial \xi}(\delta S_{ij} f_j) d\xi$$

where typically the first term is negligible and can be dropped. Other cost functions, such as the drag coefficient, lead to different adjoint boundary conditions. When a mesh perturbation procedure is defined the perturbations δS_{ij} can be directly related to the surface perturbation. Finally one obtains the cost variation as an inner product

$$\delta I \;=\; (\mathcal{G}, \delta \mathcal{F}) \;=\; \int\int \mathcal{G} \delta \mathcal{F} d\xi_1 d\xi_2$$

where $\mathcal{G}$ is the pointwise gradient, and $\mathcal{F}$ defines the surface shape.

1.3 Optimization procedure

Another key issue for successful implementation of the continuous adjoint method is the choice of an appropriate inner product for the definition of the gradient. It turns out that there is an enormous benefit from the use of a modified Sobolev gradient, which enables the generation of a sequence of smooth shapes.

The gradient $\mathcal{G}$ is generally in a lower smoothness class than the initial shape $\mathcal{F}$. Then a sequence of steps

$$\delta \mathcal{F} = -\lambda \mathcal{G}$$

progressively reduces the smoothness, leading to instability.

In order to prevent this we can introduce a weighted Sobolev inner product [14] of the form

$$\langle u, v \rangle = \int (uv + \epsilon u^{'} v^{'}) dx$$

in one dimension, where the parameter ϵ controls the smoothness. Correspondingly we define a modified gradient $\bar{\mathcal{G}}$ such that

$$\delta I =< \bar{\mathcal{G}}, \delta \mathcal{F} > .$$

In the one dimensional case $\bar{\mathcal{G}}$ is obtained by solving the smoothing equation

$$\bar{\mathcal{G}} - \frac{\partial}{\partial \xi_1} \epsilon \frac{\partial}{\partial \xi_1} \bar{\mathcal{G}} = \mathcal{G}. \tag{1.1}$$

In the multi-dimensional case the smoothing is applied in product form. Finally we set

$$\delta \mathcal{F} = -\lambda \bar{\mathcal{G}} \tag{1.2}$$

with the result that

$$\delta I = -\lambda < \bar{\mathcal{G}}, \bar{\mathcal{G}} > \quad < 0,$$

unless $\bar{\mathcal{G}} = 0$, and correspondingly $\mathcal{G} = 0$.

The implicit smoothing procedure acts as a preconditioner which allows the use of much larger steps for the search procedure and leads to a large reduction in the number of design iterations needed for convergence.

1.3.1 Outline of the design procedure

The design procedure can finally be summarized as follows:

1. Solve the flow equations for ρ, u_1, u_2, u_3, p.
2. Solve the adjoint equations for ψ subject to appropriate boundary conditions.
3. Evaluate $\mathcal{G}$ and calculate the corresponding Sobolev gradient $\bar{\mathcal{G}}$.
4. Project $\bar{\mathcal{G}}$ into an allowable subspace that satisfies any geometric constraints.
5. Update the shape based on the direction of steepest descent.
6. Return to 1 until convergence is reached.

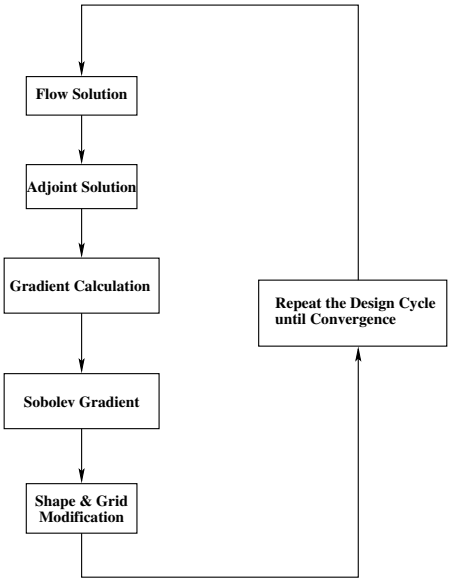

Fig. 1.1. Design cycle

Practical implementation of the design method relies heavily upon fast and accurate solvers for both the state (w) and co-state (ψ) systems. The result obtained in Section 1.4 have been obtained using well-validated software for the solution of the Euler and Navier-Stokes equations developed over the course of many years [5, 15, 16]. For inverse design the lift is fixed by the target pressure. In drag minimization it is also appropriate to fix the lift coefficient, because the induced drag is a major fraction of the total drag, and this could be reduced simply by reducing the lift. Therefore the angle of attack is adjusted during each flow solution to force a specified lift coefficient to be attained, and the influence of variations of the angle of attack is included

in the calculation of the gradient. The vortex drag also depends on the span loading, which may be constrained by other considerations such as structural loading or buffet onset. Consequently, the option is provided to force the span loading by adjusting the twist distribution as well as the angle of attack during the flow solution.

The design procedure has been implemented in the computer programs Syn88 and Syn107 for three-dimensional wing-fuselage design using the Euler and RANS equations respectively on structured meshes. Both codes include automatic mesh generation. The method has also been implemented for unstructured meshes in the computer program Synplane, which treats complete aircraft.

1.4 Case studies

1.4.1 B747 Euler planform result

The shape changes in the section needed to improve the transonic wing design are quite small. However, in order to obtain a true optimum design larger scale changes such as changes in the wing planform (sweepback, span, chord, section thickness, and taper) should be considered. Because these directly affect the structure weight, a meaningful result can only be obtained by considering a cost function that accounts for both the aerodynamic characteristics and the weight.

In references [8, 11, 17] the cost function is defined as

$$I = \alpha_1 C_D + \alpha_2 \frac{1}{2} \int_{\mathcal{B}} (p - p_d)^2 dS + \alpha_3 C_W,$$

where $C_W \equiv \frac{W}{q_\infty S_{ref}}$ is a dimensionless measure of the wing weight, which can be estimated either from statistical formulas, or from a simple analysis of a representative structure, allowing for failure modes such as panel buckling. The coefficient α_2 is introduced to provide the designer some control over the pressure distribution, while the relative importance of drag and weight are represented by the coefficients α_1 and α_3. By varying these it is possible to calculate the Pareto front of designs which have the least weight for a given drag coefficient, or the least drag coefficient for a given weight. The relative importance of these can be estimated from the Breguet range equation;

$$\begin{aligned} \frac{\delta R}{R} &= -\left(\frac{\delta C_D}{C_D} + \frac{1}{log \frac{W_1}{W_2}} \frac{\delta W_2}{W_2} \right) \\ &= -\left(\frac{\delta C_D}{C_D} + \frac{1}{log \frac{W_1}{W_2}} \frac{\delta C_W}{\frac{W_2}{q_\infty S_{ref}}} \right). \end{aligned}$$

Figure 1.2 shows the Pareto front obtained from a study of the Boeing 747 wing [17], in which the flow was modeled by the Euler equations. The wing

planform and section were varied simultaneously, with the planform defined by six parameters; sweepback, span, the chord at three span stations, and wing thickness. The weight was estimated from an analysis of the section thickness required in the structural box. The figure also shows the point on the Pareto front when $\frac{\alpha_3}{\alpha_1}$ is chosen such that the range of the aircraft is maximized. The optimum wing, as illustrated in figure 1.3, has a larger span, a lower sweep angle, and a thicker wing section in the inboard part of the wing. The increase in span leads to a reduction in the induced drag, while the section shape changes keep the shock drag low. At the same time the lower sweep angle and thicker wing section reduce the structural weight. Overall, the optimum wing improves both aerodynamic performance and structural weight. The drag coefficient is reduced from 108 counts to 87 counts (19%), while the weight factor C_W is reduced from 455 counts to 450 counts (1%).

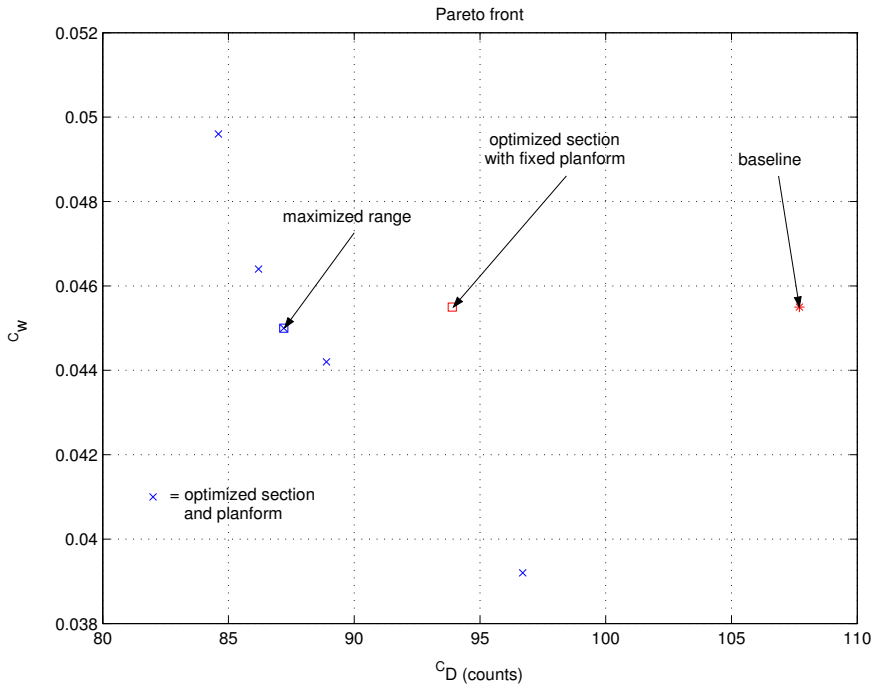

Fig. 1.2. Pareto front of section and planform modifications

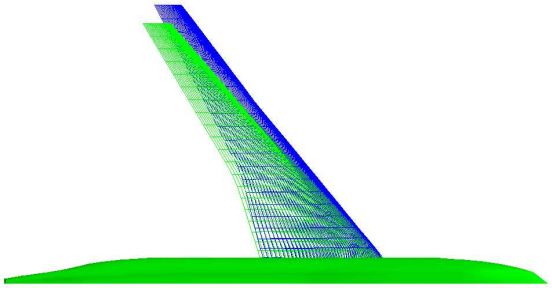

Fig. 1.3. Superposition of the baseline (green) and the optimized section-and-planform (blue) geometries of Boeing 747. The redesigned geometry has a longer span, a lower sweep angle, and thicker wing sections, improving both aerodynamic and structural performances. The optimization is performed at Mach .87 and fixed C_L .42, where $\frac{\alpha_3}{\alpha_1}$ is chosen to maximize the range of the aircraft.

1.4.2 Super B747

In order to explore the limits of attainable performance the B747 wing has been replaced by a completely new wing to produce a "Super B747". An initial design was created by blending supercritical wing sections obtained from other optimizations to the optimum planform which was found in the planform study described in the previous section. Then the RANS optimization code Syn107 was used to obtain minimize drag over 3 design points at Mach .78, .85, and .87, shown in figures 1.4 (a)-(c) with a fixed lift coefficient of .45 for the exposed wing, corresponding to a lift coefficient of about .52 when the fuselage lift is included. Because the new wing sections are significantly thicker, the new wing is estimated to be 12,000 pounds lighter than the baseline B747 wing as shown in table 1.1. At the same time the drag is reduced over the entire range from Mach .78 to .90 with a maximum benefit of 25 counts at Mach .87, as shown in figure 1.4 (d). Figure 1.5 and table 1.2 display the lift-drag polar at Mach .86. The drag coefficient of the Super B747 is 142 counts at a lift coefficient of .5, whereas the baseline B747 has the same drag at a lift coefficient of .45. This represents improvement in L/D of more than 10 percent. In combination with the reduction in wing weight and an increase in fuel volume due to the thicker wing section, this should lead to an increase in range which is substantially more than 10 percent.

Table 1.1. Comparison between Baseline B747 and Super B747 at Mach .86

	C_L	C_D counts	C_W counts
Boeing 747	.45	141.3 (107.0 pressure, 34.3 viscous)	499 (82,550 lbs)
Super B747	.50	141.9 (104.8 pressure, 37.1 viscous)	427 (70,620 lbs)

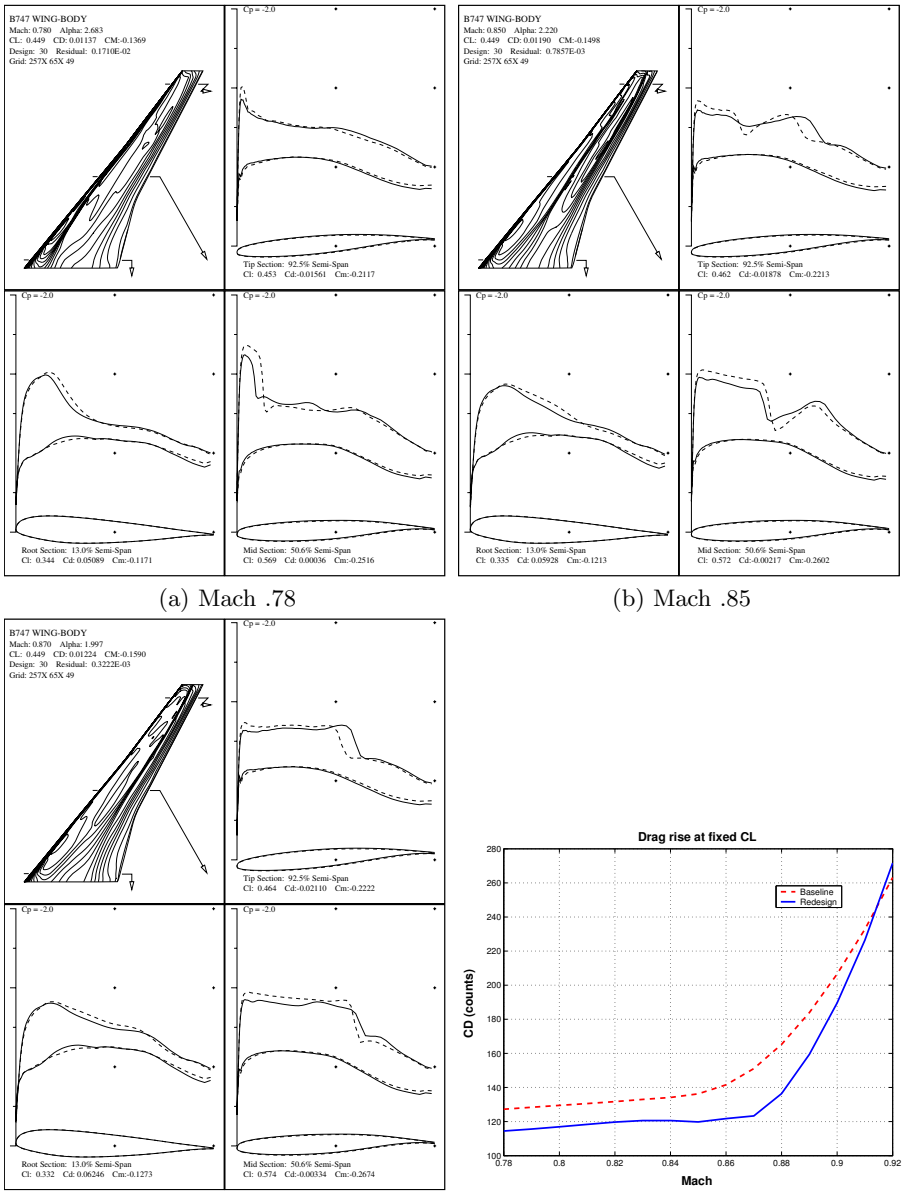

(a) Mach .78 (b) Mach .85

(c) Mach .87 (d) Drag Vs. Mach number

Fig. 1.4. (a)-(c): Super B747 at Mach .78, .85, and .87 respectively. Dash line represents shape and pressure distribution of the initial configuration. Solid line represents those of the redesigned configuration. **(d)**: Drag Vs. Mach number of Super B747.

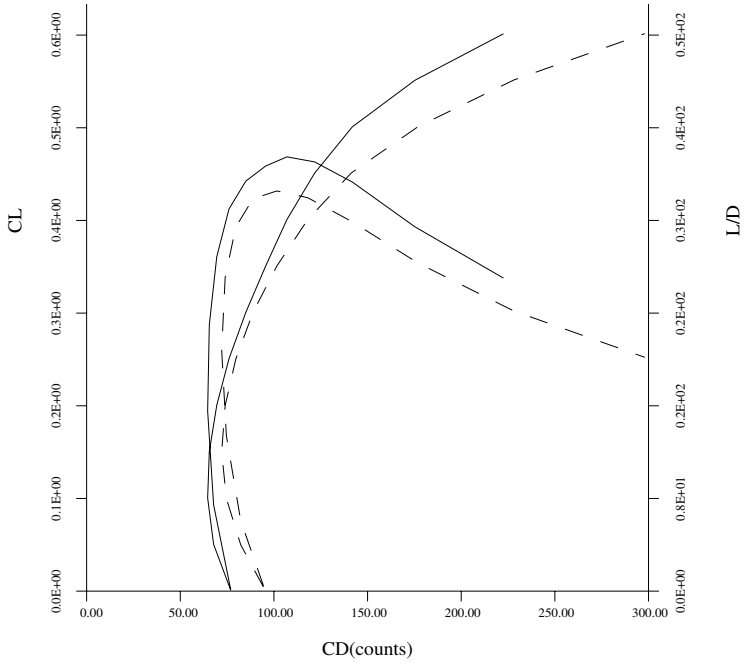

Fig. 1.5. Drag Polars of Baseline and Super B747 at Mach .86. (Solid-line represents Super B747. Dash-line represents Baseline B747.)

Table 1.2. Comparison of drag polar; B747 Vs. Super B747

Boeing 747		Super B747	
C_L	C_D	C_L	C_D
0.0045	94.3970	0.0009	76.9489
0.0500	82.2739	0.0505	67.8010
0.1000	74.6195	0.1005	64.6147
0.1501	72.1087	0.1506	65.5073
0.2002	73.9661	0.2006	69.4840
0.2503	79.6424	0.2507	76.0041
0.3005	88.7551	0.3008	84.9889
0.3507	101.5293	0.3509	95.6117
0.4009	118.0487	0.4010	106.9625
0.4512	**141.2927**	0.4510	121.7183
0.5014	177.0959	**0.5010**	**141.8675**
0.5516	228.1786	0.5512	175.2569
0.6016	298.0458	0.6014	222.5459

(C_D in counts)

Note equal drag of the baseline B747 at C_L .45 and the Super B747 at C_L .5.

1.4.3 Shape optimization for a transonic business Jet

The unstructured design method has also been applied to several complete aircraft configurations. The results for a business jet are shown in figures 1.6 (a) and (b). There is a strong shock over the out board wing sections of the initial configuration, which is essentially eliminated by the redesign. The drag was reduced from 235 counts to 215 counts in about 8 design cycles. The lift was constrained at 0.4 by perturbing the angle of attack. Further, the original thickness of the wing was maintained during the design process ensuring that fuel volume and structural integrity will be maintained by the redesigned shape. Thickness constraints on the wing were imposed on cutting planes along the span of the wing and by transferring the constrained shape movement back to the nodes of the surface triangulation.

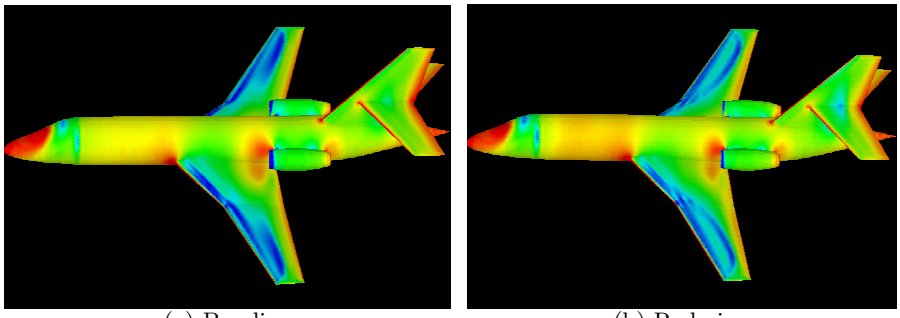

(a) Baseline (b) Redesign

Fig. 1.6. Density contours for a business jet at $M = 0.8$, $\alpha = 2^o$

1.5 Conclusion

The accumulated experience of the last decade suggests that most existing aircraft which cruise at transonic speeds are amenable to a drag reduction of the order of 3 to 5 percent, or an increase in the drag rise Mach number of at least .02. These improvements can be achieved by very small shape modifications, which are too subtle to allow their determination by trial and error methods. When larger scale modifications such as planform variations or new wing sections are allowed, larger gains in the range of 5-10 percent are attainable. The potential economic benefits are substantial, considering the fuel costs of the entire airline fleet. Moreover, if one were to take full advantage of the increase in the lift to drag ratio during the design process, a smaller aircraft could be designed to perform the same task, with consequent further cost reductions. Methods of this type will provide a basis for aerodynamic designs of the future.

References

1. J. L. Lions. *Optimal Control of Systems Governed by Partial Differential Equations*. Springer-Verlag, New York, 1971. Translated by S.K. Mitter.
2. A. Jameson. Aerodynamic design via control theory. *Journal of Scientific Computing*, 3:233–260, 1988.
3. A. Jameson. Computational aerodynamics for aircraft design. *Science*, 245:361–371, July 1989.
4. J. Reuther, A. Jameson, J. Farmer, L. Martinelli, and D. Saunders. Aerodynamic shape optimization of complex aircraft configurations via an adjoint formulation. *AIAA paper 96-0094*, 34th Aerospace Sciences Meeting and Exhibit, Reno, Nevada, January 1996.
5. A. Jameson, W. Schmidt, and E. Turkel. Numerical solutions of the Euler equations by finite volume methods with Runge-Kutta time stepping schemes. *AIAA paper 81-1259*, January 1981.
6. A. Jameson and T.J. Baker. Improvements to the aircraft Euler method. *AIAA paper 87-0452*, AIAA 25th Aerospace Sciences Meeting, Reno, Nevada, January 1987.
7. T. J. Barth. Apects of unstructured grids and finite volume solvers for the Euler and Navier Stokes equations. *AIAA paper 91-0237*, AIAA Aerospace Sciences Meeting, Reno, NV, January 1991.
8. K. Leoviriyakit and A. Jameson. Aerodynamic shape optimization of wings including planform variations. *AIAA paper 2003-0210*, 41^{st} Aerospace Sciences Meeting & Exhibit, Reno, Nevada, January 2003.
9. A. Jameson. A perspective on computational algorithms for aerodynamic analysis and design. *Progress in Aerospace Sciences*, 37:197–243, 2001.
10. S. Kim, J. J. Alonso, and A. Jameson. Design optimization of high-lift configurations using a viscous continuous adjoint method. *AIAA paper 2002-0844*, AIAA 40th Aerospace Sciences Meeting & Exhibit, Reno, NV, January 2002.
11. K. Leoviriyakit, S. Kim, and A. Jameson. Viscous aerodynamic shape optimization of wings including planform variables. *AIAA paper 2003-3498*, 21^{st} Applied Aerodynamics Conference, Orlando, Florida, June 23-26 2003.
12. A. Jameson and S. Kim. Reduction of the adjoint gradient formula in the continuous limit. *AIAA paper 2003-0844*, AIAA 41st Aerospace Sciences Meeting & Exhibit, Reno, NV, January 2003.
13. A. Jameson, Sriram, and L. Martinelli. An unstructured adjoint method for transonic flows. *AIAA paper*, 16^{th} AIAA CFD Conference, Orlando, FL, June 2003.
14. A. Jameson, L. Martinelli, and J. Vassberg. Reduction of the adjoint gradient formula in the continuous limit. *AIAA paper*, 41^{st} AIAA Aerospace Sciences Meeting, Reno, NV, January 2003.
15. L. Martinelli and A. Jameson. Validation of a multigrid method for the Reynolds averaged equations. *AIAA paper 88-0414*, 1988.
16. S. Tatsumi, L. Martinelli, and A. Jameson. A new high resolution scheme for compressible viscous flows with shocks. *AIAA paper* To Appear, AIAA 33nd Aerospace Sciences Meeting, Reno, Nevada, January 1995.
17. K. Leoviriyakit and A. Jameson. Aero-structural wing planform optimization. Reno, Nevada, January 2004. Proceedings of the 42^{st} Aerospace Sciences Meeting & Exhibit.